

Fermi National Accelerator Laboratory

FERMILAB-Conf-87/108-T

June, 1987

Heavy Flavour Production and Colour Coherence in Hadronic Scattering

R. K. Ellis

Fermi National Accelerator Laboratory

P. O. Box 500, Batavia, Illinois 60510

Abstract

Two recent advances in perturbative QCD are described. Firstly, the theory of heavy flavour production is reviewed. Detailed results of the simple perturbative QCD formula are presented. It is argued that there are significant advantages in hadro-producing both charm and bottom quarks with pions rather than with protons. Secondly, the implications of colour coherence for hadronic hard scattering events are discussed. It is shown that soft radiation in hadron-hadron scattering can be represented as an incoherent sum of terms, subject to a dynamical angular ordering constraint. All the elements necessary to set up a shower Monte Carlo are now present. The observability of the string effect in hadronic collisions at the Fermilab collider is discussed.

Extended version of a talk delivered at 'Les Rencontres de Physique de la Vallée d'Aoste', La Thuile, Italy, March 1-7, 1987.



1 Heavy flavour production

Experimental results on the hadroproduction of charmed particles are hard to interpret, because the measured cross-sections appear to vary widely between experiments^[1]. Moreover the measured differential distributions are not always explicable within the context of the simple perturbative QCD picture. With the advent of new experiments it is to be hoped that the hadroproduction of charmed particles will pass from this adolescent phase, to a full maturity in which it will reveal its strength both as a probe of perturbative and non-perturbative Quantum Chromodynamics and as a copious source of charmed particles. The hadroproduction of bottom quarks on the other hand is still in its infancy^[2]. The high-statistics obtained^[3] for the photoproduction of charm in Fermilab experiment E-691 provide great encouragement for experiments aimed at the hadroproduction of charm and beauty, such as Fermilab experiment E-769 which uses similar detection techniques. Another reason for great experimental interest in bottom and charm production at collider energies is that it has become apparent that these processes provide significant backgrounds in the search for new flavours, such as the top.

These experimental considerations have provided motivation for attempts to put heavy flavour production on a more solid theoretical footing. The recent theoretical progress^[4,5,6] can be summarized as follows. It is now believed that the dominant parton reactions leading to the production of a sufficiently heavy quark Q are

$$\begin{aligned} (a) \quad & q(p_1) + \bar{q}(p_2) \rightarrow Q(p_3) + \bar{Q}(p_4) \\ (b) \quad & g(p_1) + g(p_2) \rightarrow Q(p_3) + \bar{Q}(p_4) , \end{aligned} \tag{1}$$

where the four momenta of the partons are given in brackets. The invariant matrix elements squared for processes (a) and (b) have been available in the literature for some time^[10,11,12] and are given by

$$\overline{\sum} |M^{q\bar{q} \rightarrow Q\bar{Q}}(p_1, p_2, p_3, p_4)|^2 = \frac{g^4 V}{2N^2} \left(\frac{\{13\}^2 + \{23\}^2}{\{12\}^2} + \frac{m^2}{\{12\}} \right) \tag{2}$$

$$\begin{aligned} \overline{\sum} |M^{gg \rightarrow Q\bar{Q}}(p_1, p_2, p_3, p_4)|^2 = \\ \frac{g^4}{2VN} \left(\frac{V}{\{13\}\{23\}} - \frac{2N^2}{\{12\}^2} \right) \left(\{13\}^2 + \{23\}^2 + 2m^2\{12\} - \frac{m^4\{12\}^2}{\{13\}\{23\}} \right) , \end{aligned} \tag{3}$$

where the dependence on the $SU(N)$ color group is shown explicitly, ($V = N^2 - 1$, $N = 3$) and m is the mass of the produced heavy quark Q . The matrix elements squared in Eqs. (2,3) have been summed and averaged over initial and final colours and spins, (as indicated by $\overline{\sum}$). For brevity, we have introduced the notation for the scalar product of two four-momenta.

$$p_i \cdot p_j = \{ij\} \tag{4}$$

The transverse momentum of the heavy quark or antiquark produced by the processes of Eq. (1) is, on the average, of the order of its mass, whereas the transverse momentum of the quark-antiquark pair is small. In addition the cross section for the production of charmed particles is predominantly central^[6]. To check that this conclusion is not vitiated by higher order corrections, in ref.[6] the leading $O(\alpha_s^3)$ correction at large x_F was calculated. It was shown that for the case of charmed quarks this contribution gives a negative correction to the processes in Eq. (1) after factorisation. Although much progress^[7,8,9] in the calculation of $O(\alpha_s^3)$ corrections to heavy quark production has been made

a full calculation is still lacking. The theoretical arguments summarized above do not address the issue of whether the charmed quark is sufficiently heavy that the hadroproduction of charmed hadrons in all regions of phase space is well described by only processes (a) and (b) and their perturbative corrections.

We now address the question of the relative efficacy of pion and proton beams in producing heavy quarks, which is of interest to plan experiments^[13,14]. In Fig. 1 we show a comparison of the cross-sections for the production of charmed quarks by beams of pions and protons. We have calculated rates for heavy flavour production via the elementary two-body processes (a) and (b) using the pion structure functions of Owens^[15] and, for consistency, the proton structure functions of Duke and Owens.^[16] For the strong coupling constant we use the standard one-loop expression

$$1/\alpha_s(Q^2) = \frac{27}{12\pi} \log \frac{Q^2}{\Lambda^2} - \frac{1}{6\pi} \sum_{i=c,b,\dots} \theta(Q^2 - 4m_i^2) \log(Q^2/4m_i^2) \quad (5)$$

with $\Lambda=200$ MeV. In both the structure functions and the strong coupling constant we take $Q^2 = 4m_c^2$. The cross sections are calculated for an "isoscalar nucleon" $N \equiv (p+n)/2$. The results we present refer to the cross sections for producing *either* a quark *or* an antiquark (*not summed*). This must be kept in mind in comparing with experimental results. Furthermore, the experimental results are for the production of particular hadrons containing heavy quarks, whereas our results are for the production of heavy quarks. Thus the branching fraction of heavy quark decays to the observed hadron containing that quark must also be included in the comparison.

The integrated cross sections for charm production in πN and pN collisions are shown in Fig. 1 for charmed quark masses $m_c = 1.2, 1.8$ GeV. There is considerable sensitivity to the quark mass: the rates differ by nearly an order of magnitude for the two choices. This sensitivity is largely due to the rapid growth of the gluon distribution function as we proceed to lower values of x . In the forward region ($x_F > 0.2$), pion beams produce charm at about twice the rate of proton beams, as shown in Fig. 2. This can be seen in detail in Fig. 3, where the distribution in x_F is shown for pion and proton beams of momentum of 250 GeV, appropriate for experiment E-769. The advantage of the pion beam for charm production lies principally in the harder gluon distribution, proportional to $(1-x)^{3.1}$ versus $(1-x)^6$ for the proton, not in the contribution of valence antiquarks. The stiffer gluon distribution function leads to greater production in the forward direction. Fig. 4 shows the distribution in p_T^2 in the forward region at the same beam momentum.

Turning now to the production of bottom quarks, the integrated cross sections in nanobarns for πN and pN collisions are shown in Fig. 5 for bottom quark masses $m_b = 4.7, 5.3$ GeV, $Q^2 = 4m_b^2$. As was the case for charm, there is considerable sensitivity to the quark mass, now at the level of a factor of three to four. In both cases, there is a significant advantage for the pion beam. This advantage is accentuated when attention is restricted to forward production ($x_F > 0.2$), as shown in Fig. 6. For pN collisions the gluon fusion mechanism (b) is dominant, except at the lowest energies. For πN collisions, the situation is quite different. The $q\bar{q}$ annihilation process (a) is pre-eminent, with gluon fusion contributing significantly only at the highest energies. The prominence of mechanism (a) is of course due to presence of valence antiquarks in the pion. Fig 7 shows the x_F distribution at a beam momentum of 250 GeV. Lastly in Fig. 8 we show the distribution in p_T^2 in the region $x_F > 0.2$ at the same beam momentum.

Thus for experiments sensitive to forward production of heavy flavours, we find that pion beams hold an advantage over proton beams for the production of both charm and bottom. This in part because the heavy flavour cross-sections are larger, but also because the πN total cross-section which is smaller than the pN total cross-section will provide a smaller background to the search for heavy flavours. The general conclusion is that choosing a pion beam to enhance the prospects of a search for bottom quarks will not compromise the yield of charmed particles.

2 Colour Coherence in Jet Physics

Because of the presence of coloured constituents in both the initial and final states, the study of hard processes in hadron-hadron collisions has proved more complicated, experimentally and theoretically, than in electron-positron annihilation. In this report the inclusion of the colour coherence of soft radiation is described for the case of hadron-hadron scattering. This analysis puts jet physics on essentially the same theoretical footing as e^+e^- annihilation. It is known that large terms associated with collinear gluon emission can be deduced from the factorisation of mass singularities, but those arising from soft non-collinear gluon emission cannot yet be fully derived from general principles. However, the leading logarithmic contributions in perturbative QCD can be represented by treelike graphs, corresponding to a parton cascade in which the characteristic parton virtuality decreases as one moves away from the hard subprocess^[17]. After averaging over azimuthal angles with respect to the hard parton directions, the leading effect of soft gluon interference (coherence) is a reduction of the available phase space for the cascade to an angular-ordered region^[17,18,19,20].

For the case of three jet events in e^+e^- annihilation the coherence of the radiation from the hard partons leads to the string effect^[21,22]. In the language of perturbative QCD, the string effect is a result of constructive and destructive interference. Of course, it is entirely unremarkable that such interference effects should be observed in quantum field theory. However, it is interesting to note that the experimental evidence indicates that such interference effects survive the hadronisation process, a phenomenon which the authors of ref.(22) call local parton-hadron duality.

At sufficiently high energy, the colour structure of a hadron-hadron collision in which a hard scattering occurs will also determine the pattern of associated radiation. Because the distribution of this radiation is not significantly altered by hadronisation the observed pattern of the hadrons which lie between the jets will depend on the colour of the partons participating in the hard scatter. At the end of this section we shall examine whether the string effect is observable in hadronic scattering at Tevatron energies.

In the case of radiation from outgoing partons, which have timelike virtualities, the angular ordering is such that the emission angles of soft gluons decrease as the parton cascade evolves from the hard subprocess towards lower virtualities. It has recently been discovered^[23,24] that the soft radiation from incoming, spacelike partons should follow an analogous ordering: in this case the angles of emission increase as one moves from the initial hadrons to the hard subprocess. The parton-cascade interpretation of the leading perturbative contributions suggests the Monte Carlo simulation technique for their numerical evaluation. The Monte Carlo method also permits one to follow easily the flow of colour in the cascade, at least to leading order in N , since to this order the colours of all external lines may be traced continuously through the corresponding tree diagram. Finally, in a Monte Carlo

simulation it is straightforward to combine the perturbative parton cascade with a nonperturbative model for the conversion of parton configurations into hadrons (hadronization) at any desired scale of virtuality.

Monte Carlo programs including coherence via angular ordering are already available for the case of final-state cascades (timelike parton evolution) such as those in e^+e^- annihilation [25,26]. Here the largest angle is the initial one between the quark and antiquark at the photon vertex. The resulting colour and momentum structure of the parton cascade is particularly simple, and, when combined with colour- and momentum-conserving models of hadronization [27], accounts for many features of the experimental data[28].

We first illustrate the derivation of the angle ordered approximation in the process $e^+e^- \rightarrow q\bar{q}g$. Soft gluons are emitted only inside certain angular regions around the directions of the hard partons q , \bar{q} and g . We introduce the angular variables $\zeta_i = 1 - \cos\theta_i$, where θ_i is the angle between the soft gluon and the hard parton i , and $\zeta_{ij} = 1 - \cos\theta_{ij}$ where θ_{ij} is the angle between hard partons i and j . In terms of these variables the eikonal factor which describes the emission of soft radiation may be written,

$$[ij] = g^2 \frac{p_i \cdot p_j}{p_i \cdot k k \cdot p_j} = \frac{g^2}{|k|^2} \frac{\zeta_{ij}}{\zeta_i \zeta_j} = \left(\frac{g^2}{2|k|^2} \left\{ \frac{\zeta_{ij}}{\zeta_i \zeta_j} + \frac{1}{\zeta_i} - \frac{1}{\zeta_j} \right\} \right) + (i \leftrightarrow j) \quad (6)$$

where $|k|$ represents the energy of the soft gluon. The expression in braces contains the collinear pole at $\zeta_i = 0$ but not that at $\zeta_j = 0$. Furthermore, when averaged over the azimuthal angle ϕ_i around the direction of hard parton i , it vanishes outside the cone $\zeta_i = \zeta_{ij}$. In fact[19,22],

$$\int \frac{d\phi_i}{2\pi} \left\{ \frac{\zeta_{ij}}{\zeta_i \zeta_j} + \frac{1}{\zeta_i} - \frac{1}{\zeta_j} \right\} = \frac{2}{\zeta_i} \Theta(\zeta_{ij} - \zeta_i) \quad (7)$$

Hence, averaging each term with respect to azimuth around its direction of singularity, we may write,

$$[ij] = \frac{g^2}{|k|^2 \zeta_i} \Theta(\zeta_{ij} - \zeta_i) + \frac{g^2}{|k|^2 \zeta_j} \Theta(\zeta_{ij} - \zeta_j) \quad (8)$$

Eq.(8) has the same form as the incoherent radiation emission result but with a dynamically imposed angular constraint on the phase space.

For a simple hard subprocess such as $q\bar{q} \rightarrow Z, W^+, \text{ or } W^-$ ($Z, W^+, \text{ or } W^-$ production in hadron-hadron collisions) the perturbative analysis is entirely analogous to the case of e^+e^- annihilation described above. The starting angle for the backward cascade is that between the quark and antiquark at the Z or W vertex. Moreover the colour flow at the elementary hard vertex is again simple, and therefore the colour structure of the parton cascade is easily recovered.

The situation is more involved for processes involving both incoming and outgoing coloured partons, such as the production of two hard jets in a hadron-hadron collision, for which the elementary hard subprocess (h) is $2 \rightarrow 2$ parton scattering,

$$(h) \quad \text{parton}(p_1) + \text{parton}(p_2) \rightarrow \text{parton}(p_3) + \text{parton}(p_4) \quad (9)$$

In this case there is interference between soft gluon emissions from spacelike and timelike lines and it is not obvious which angles should be used to initiate the various parton cascades. Furthermore the hard matrix element squared $|M^{(h)}|^2$ receives contributions from different colour flow diagrams, each one leading to a different colour structure for the produced multiparton state. In order to extend the

Monte Carlo simulation with coherence to such processes, one must find the correct initial angles and weights corresponding to each colour flow contribution.

The generalisation of the procedure for e^+e^- annihilation to the case of parton-parton scattering is straightforward^[30]. We start from the known^[9,8] exact expression for the matrix element squared $|M^{(H)}|^2$ for the general hard $2 \rightarrow 3$ parton process (H):

$$(H) \quad \text{parton}(p_1) + \text{parton}(p_2) \rightarrow \text{parton}(p_3) + \text{parton}(p_4) + \text{gluon}(k) \quad (10)$$

We then take the soft limit for the gluon momentum ($k \rightarrow 0$) in $|M^{(H)}|^2$ so that the process (H) reduces to the process (h) with a soft gluon emitted from each hard parton i . As discussed in Refs.[17,22] the soft momentum dependence factorizes into the eikonal factors,

$$[ij] \equiv g^2 \frac{p_i \cdot p_j}{p_i \cdot k \ k \cdot p_j} \quad (11)$$

so that we may write,

$$\overline{|M^{(H)}|^2} \rightarrow \sum_{ij} [ij] A_{ij}^{(h)} \quad (12)$$

where the coefficients $A_{ij}^{(h)}$ are functions of the kinematic invariants of the $2 \rightarrow 2$ process (h) in Eq.(9).

After appropriate azimuthal averaging, the eikonal factors in Eq. (11), reduce to sums of Θ -functions^[17,22] in the angular variables θ_i and θ_{ij} , the latter being the angle between the two hard partons i and j . These Θ -functions define the available phase space in θ_i for the various contributions, and consequently the largest initial angle for the radiation emitted from the parton i .

The main result is very simple: around each one of the four hard partons in the elementary process (h) there is a cone bounded by the nearest other hard parton ($\theta_i < \theta_{ij}$), in which the soft gluon bremsstrahlung is simply given by,

$$\overline{|M^{(H)}|^2} \rightarrow \frac{2g^2 C_i}{|k|^2} \frac{1}{(1 - \cos \theta_i)} \overline{|M^{(h)}|^2} \quad (13)$$

Here $C_i = C_F$ for a quark, C_A for a gluon, ($C_A = N = 3$, $C_F = (N^2 - 1)/(2N)$). Only these four contributions are collinear singular as $\theta_i \rightarrow 0$.

The full results for QCD including the azimuthal averaging procedure are given in Ref.(30). The implementation of the angular averaging using Eq.(8) is straightforward and we do not report it here. Instead we present the full results from which the angular averaged results can be obtained. In QCD there are four two-to-three parton scattering processes which we must consider in order g^6 ,

$$\begin{aligned} (A) \quad & q(p_1) + q'(p_2) \rightarrow q(p_3) + q'(p_4) + g(k) \\ (B) \quad & q(p_1) + q(p_2) \rightarrow q(p_3) + q(p_4) + g(k) \\ (C) \quad & q(p_1) + \bar{q}(p_2) \rightarrow g(p_3) + g(p_4) + g(k) \\ (D) \quad & g(p_1) + g(p_2) \rightarrow g(p_3) + g(p_4) + g(k) \end{aligned} \quad (14)$$

All other matrix elements for two-to-three parton processes may be obtained by crossing. It will be useful to consider also the W production process with gluon radiation,

$$(E) \quad q(p_1) + \bar{q}(p_2) \rightarrow W(p_3) + g(p_4) + g(k) \quad (15)$$

The exact spin and colour averaged matrix elements squared for the processes ($A - E$) have been given in refs.(9,8,31). In the soft limit $k \rightarrow 0$ the matrix element for process (A) becomes,

$$\overline{\sum} |M^{(A)}|^2 = H^{(a)}(s, t, u) \left\{ 2C_F ([14] + [23]) + \frac{1}{N} [12; 34] \right\} \quad (16)$$

where the dependence on the $SU(N)$ colour group is shown explicitly and the eikonal factor $[ij]$ is defined in Eq.(11). For simplicity we have defined the following frequently occurring sum of eikonal terms,

$$[12; 34] = 2[12] + 2[34] - [13] - [14] - [23] - [24] \quad (17)$$

which has no collinear singularities, and

$$s = (p_1 + p_2)^2, \quad t = (p_1 - p_3)^2, \quad u = (p_1 - p_4)^2, \quad (18)$$

The $2 \rightarrow 2$ matrix element squared $H^{(a)}$ is given in Table I.

a) $q(p_1) + q'(p_2) \rightarrow q(p_3) + q'(p_4)$ $\overline{\sum} M^{(a)} ^2 = H^{(a)}(s, t, u)$	$\frac{g^4 C_F}{N} \left(\frac{s^2 + u^2}{t^2} \right)$
b) $q(p_1) + q(p_2) \rightarrow q(p_3) + q(p_4)$ $\overline{\sum} M^{(b)} ^2 = H^{(b)}(s, t, u)$ $H_1^{(b)}(s, t, u)$	$\frac{g^4 C_F}{N} \left(\frac{s^2 + u^2}{t^2} \right) + \frac{g^4 C_F}{N} \left(\frac{s^2 + t^2}{u^2} \right) - \frac{2g^4 C_F}{N^2} \left(\frac{s^2}{tu} \right)$ $\frac{g^4 C_F}{N} \left(\frac{s^2}{tu} \right)$
c) $q(p_1) + \bar{q}(p_2) \rightarrow g(p_3) + g(p_4)$ $\overline{\sum} M^{(c)} ^2 = H^{(c)}(s, t, u)$ $H_1^{(c)}(s, t, u)$ $H_2^{(c)}(s, t, u)$	$g^4 C_F (t^2 + u^2) \left[\left(1 - \frac{1}{N^2} \right) \frac{1}{tu} - \frac{2}{s^2} \right]$ $g^4 \frac{N}{4} (t^2 + u^2) \left[\left(1 - \frac{2}{N^2} \right) \frac{1}{tu} - \frac{2}{s^2} \right]$ $g^4 \frac{N}{4} (t^2 - u^2) \left[\frac{1}{tu} - \frac{2}{s^2} \right]$
d) $g(p_1) + g(p_2) \rightarrow g(p_3) + g(p_4)$ $\overline{\sum} M^{(d)} ^2 = H^{(d)}(s, t, u)$ $H_1^{(d)}(s, t, u)$	$\frac{4g^4 N^2}{(N^2 - 1)} \left[3 - \frac{ut}{s^2} - \frac{us}{t^2} - \frac{st}{u^2} \right]$ $\frac{2g^4 N^2}{3(N^2 - 1)} \left[\frac{st}{u^2} + \frac{su}{t^2} - 2\frac{tu}{s^2} - 3\frac{s^2}{ut} + 3 \right]$

Table I. Spin and colour averaged matrix elements squared for $2 \rightarrow 2$ processes and the auxiliary functions necessary to describe the soft limit of $2 \rightarrow 3$ processes. $s = (p_1 + p_2)^2$, $t = (p_1 - p_3)^2$ and $u = (p_2 - p_3)^2$.

In the limit $k \rightarrow 0$ the matrix element squared for process B may be written in the form,

$$\begin{aligned} \overline{\sum} |M^{(B)}|^2 \rightarrow & \left(H^{(a)}(s, t, u) - \frac{1}{N} H_1^{(b)}(s, t, u) \right) \left\{ 2C_F ([14] + [23]) \right\} \\ & + \left(H^{(a)}(s, u, t) - \frac{1}{N} H_1^{(b)}(s, u, t) \right) \left\{ 2C_F ([13] + [24]) \right\} \\ & + \left(H^{(a)}(s, t, u) + H^{(a)}(s, u, t) - \left(N + \frac{1}{N} \right) H_1^{(b)}(s, t, u) \right) \left\{ \frac{1}{N} [12; 34] \right\} \end{aligned} \quad (19)$$

where the auxiliary function $H_1^{(b)}$ is given in Table I.

For process (C) the exact result has been given in ref.(9). In the soft limit $k \rightarrow 0$ we obtain

$$\begin{aligned} \overline{\sum} |M^{(C)}|^2 \rightarrow & \\ & H^{(c)}(s, t, u) \{2C_F[12] + 2C_A[34]\} \\ & - H_1^{(c)}(s, t, u) \{2C_F[12; 34]\} + H_2^{(c)}(s, t, u) \{2C_F([14] + [23] - [13] - [24])\} \end{aligned} \quad (20)$$

$H^{(c)}$ is the invariant matrix element squared for the process $q + \bar{q} \rightarrow g + g$, and is given together with $H_1^{(c)}, H_2^{(c)}$ which are the auxiliary functions¹ in Table I.

For process (D) we obtain,

$$\begin{aligned} \overline{\sum} |M^{(D)}|^2 \rightarrow & \\ & H^{(d)}(s, t, u) \left\{ \frac{2}{3} C_A ([12] + [34] + [13] + [14] + [23] + [24]) \right\} \\ & + C_A \left\{ H_1^{(d)}(s, t, u) ([12] + [34]) + H_1^{(d)}(t, s, u) ([13] + [24]) + H_1^{(d)}(u, t, s) ([14] + [23]) \right\} \end{aligned} \quad (21)$$

where $H^{(d)}$ is the $2 \rightarrow 2$ gluon scattering matrix element squared given in Table I together with the auxiliary function $H_1^{(d)}$, which satisfies the relation,

$$H_1^{(d)}(s, t, u) + H_1^{(d)}(t, s, u) + H_1^{(d)}(u, t, s) = 0 \quad (22)$$

Finally, for the W production process (E) the matrix element squared is given in the limit $k \rightarrow 0$ by,

$$\overline{\sum} |M^{q\bar{q} \rightarrow Wg}|^2 = \left\{ 2C_F[12] + C_A([14] + [24] - [12]) \right\} H^{q\bar{q} \rightarrow Wg}(s, t, u) \quad (23)$$

where,

$$H^{q\bar{q} \rightarrow Wg}(s, t, u) = \frac{2g_W^2 g^2 C_F}{N} \left(\frac{u}{t} + \frac{t}{u} + \frac{2s(s+t+u)}{tu} \right) \quad (24)$$

is the $q\bar{q} \rightarrow Wg$ hard scattering matrix element squared.

We have considered the soft gluon limits of the parton parton scattering processes (Eq.(14,15)). The results for the soft gluon limits of all other parton scattering processes can be obtained by crossing. After appropriate azimuthal averaging our results can be written as an incoherent sum of terms for each parton. In the notation of Eqs. (12) the contribution of parton i is of the general form,

$$W_i^{(H)} = (2C_i g^2 / |k|^2 \zeta_i) \sum_{j: \theta_i < \theta_{ij}} A_{ij}^{(h)} \quad (25)$$

At least to leading order in N , this expression is positive and so may be used to define probabilities for soft gluon emission into various cones centred on the hard parton directions.

To set up a Monte Carlo simulation of multiple soft gluon emission, one can then proceed as follows. For a given $2 \rightarrow 2$ hard parton subprocess (selected according to parton densities and hard scattering cross sections at the appropriate scale), a cone for the first gluon emission from each external line is chosen according to the relative probabilities defined above. After this choice of initial conditions, parton branching proceeds independently inside each of these cones according to the usual angular-ordering algorithm^[25], leading to backward evolution of incoming parton showers and forward evolution of outgoing ones. In the large N limit this procedure should incorporate correctly all leading infrared

¹Due to a typographical error the auxiliary function $H_1^{(c)}$ is wrongly given in the published version of ref. [30]

logarithms. By replacing the soft singularity in Eq. (25) with the full Altarelli-Parisi function^[32] one can also include the leading collinear logarithms.

All the elements are therefore assembled ready to be inserted into a Monte Carlo program. Without a complete Monte Carlo event generator, including a model for the underlying event due to the beam and target fragments, it is hard to tell at what energy the effects of colour coherence should become visible. Presumably at the SSC the effects of "soft" radiation should be easily distinguishable from the minimum bias background. For example, it is to be expected that the radiation pattern associated with the production of a Higgs boson should be different depending on whether it is produced by gluon-gluon fusion or by W-W fusion^[33].

In a recent preprint^[34] it has been suggested that the effects of colour coherence should be visible in jet events at the Tevatron $p\bar{p}$ collider operating at $\sqrt{S} = 1.8$ TeV. The basic idea is that, just as in the reaction $e^+e^- \rightarrow q\bar{q}g$, the parton-parton scattering acts as a colour antenna. The distribution of soft particles between the observed jets should be determined by the overall colour structure of the event. The multiplicity of charged pions in a given solid angle $\Omega(\theta, \phi)$ is fixed by the directions and energies of the coloured partons. In the centre of mass of the parton-parton system it can be written as,

$$\pi \frac{dN}{d\Omega} = P\left(\frac{t}{s}, \frac{u}{s}; \theta, \phi\right) \frac{dN_g}{dY} \quad (26)$$

where N_g is the multiplicity of pions in a gluon jet of energy E , and P is an antenna pattern function describing the angular distribution of soft radiation. P is defined in more detail below. The derivative of N_g with respect to $Y = \log(E/\Lambda)$ describes the multiplicity of pions into the appropriate angular region^[35], and E is to be loosely identified with the transverse energy of the hard scattering. In the leading and next-to-leading logarithmic approximation N_g is given by^[18],

$$N_g(Y) \approx 0.08Y^{-c} \exp \sqrt{\frac{12Y}{\pi b_0}} \quad (27)$$

where $b_0 = (33 - 2n_f)/12\pi$ and $c = (11 + 22n_f/27)/16\pi b_0$. Following ref. [34] the normalisation has been fixed in Eq. (27) by assuming that these asymptotic formulae hold already at $E = 17$ GeV, and equating the multiplicity of charged pions from a gluon of energy E with the total charged pion multiplicity $N_{e^+e^-} = 10.3$ observed at energy $2E$ in e^+e^- annihilation^[36]. Thus we have assumed that the multiplicity of a quark jet is approximately half the multiplicity of a gluon jet^[18].

$$N_g \approx 2N_q = N_{e^+e^-} \quad (28)$$

The results use five flavours of quarks and assume $\Lambda = 0.1$ GeV. Using Eq. (27) we obtain at $E = 20, 90$ GeV respectively,

$$\frac{dN_g}{dY} \approx 5.0, \quad \frac{dN_g}{dY} \approx 8.6. \quad (29)$$

It should be stressed that the corrections to Eq.(27) are of order $O(1/\sqrt{Y})$. Thus the numerical reliability of Eqs.(27,29) in the present energy range is by no means assured. Nevertheless when combined with the plots for the antenna pattern P which we present below they allow a preliminary estimate of whether the colour coherence effects will be visible above the normal soft scattering background.

Following ref. [34] we make a conservative estimate for the background multiplicity due to soft processes, (e.g. as observed in a minimum bias events)

$$\pi \frac{dN}{d\Omega} = \frac{1}{2} \frac{dN}{d\cos\theta} = \frac{1}{2\sin^2\theta} \frac{dN^{soft}}{d\eta} \quad (30)$$

where the number of particles per unit of pseudo-rapidity can be taken to be $dN^{soft}/d\eta \approx 6$, which is about 50% higher than the value observed by the UA5 collaboration^[37] in minimum bias events at the CERN collider at $\sqrt{S}=0.9$ TeV. A crude estimate of the observability of the colour coherence effects can be obtained by assuming that the contributions given in Eq.(26,30) are incoherent and independent, and comparing their size.

The magnitude of the function P is necessary to perform the comparison. P is the antenna pattern function which is defined as the ratio of the two-to-three and two-to-two cross-sections in the soft limit,

$$P\left(\frac{t}{s}, \frac{u}{s}; \theta, \phi\right) = \frac{|k|^2}{8Ng^2} \frac{|M^{(H)}|^2}{|M^{(h)}|^2}. \quad (31)$$

where s, t and u are the kinematic variables of the two-to-two hard scatter which provides the colour antenna. The prefactor in Eq. (31) removes certain terms which are included in the definition of the multiplicity in Eq. (26).

The simplest process to consider is the production of W -bosons at the Fermilab collider. At large p_T there are two processes which contribute.

$$\begin{aligned} (i) \quad & q(p_1) + \bar{q}(p_2) \rightarrow W(p_3) + g(p_4) \\ (ii) \quad & q(p_1) + g(p_2) \rightarrow W(p_3) + q(p_4) \end{aligned} \quad (32)$$

The antenna pattern for process (i) can be obtained from Eq. (23),

$$P\left(\frac{t}{s}, \frac{u}{s}; \theta, \phi\right) = \frac{1}{8} \left(\frac{\xi_{14}}{\xi_{154}} + \frac{\xi_{24}}{\xi_{254}} - \frac{1}{N^2} \frac{\xi_{12}}{\xi_{152}} \right) \quad (33)$$

The antenna pattern for process (ii) can be obtained by performing the interchange ($2 \leftrightarrow 4$). Fig. 9 shows the antenna pattern due to processes (i) and (ii) at 90° in the parton parton centre of mass. From process (i) the radiation between the directions of incoming quark(1) and outgoing gluon(4) is equal to the radiation between the direction of the incoming antiquark(2) and the outgoing gluon(4). On the other hand the radiation due to process (ii) is large between the directions of the incoming gluon(2) and the outgoing quark(4), but much smaller between the directions of the incoming quark(1) and the outgoing quark(4). This is qualitatively in accord with the angular ordering result^[30]. At $\sqrt{S} = 1.8$ TeV the contribution of qg scattering to W production can be sizeable at moderate values of p_T . Fig. 9 suggests that it may be possible to distinguish whether a W is produced by process (i) or (ii) on an event by event basis.

In order to examine this proposition in more detail it is useful to have an idea of the number of charged particles which contribute to the asymmetry. To do this we use Eqs.(26,29). Using Fig. 9 we estimate the angular region in which the two antenna patterns differ appreciably to be $\Delta\theta = 45^\circ$. Lacking better information we also assume $\Delta\phi = \Delta\theta = 45^\circ$. Therefore at $\theta = 45^\circ$ we obtain,

$$\Delta\Omega \approx 0.14\pi. \quad (34)$$

Temporarily setting the antenna pattern P equal to one, we see using Eq.(29) that the number of particles contributing to the asymmetry is of order 0.7 for $p_T = 20$ GeV and 1.2 for $p_T = 90$ GeV. These numbers could be underestimates. The angular range in ϕ could be larger and the useful angular range in θ might be increased by moving away from 90° scattering. Nevertheless, with such

small numbers of particles involved, the possibility for confusion of processes (i) and (ii) due to fluctuations must be large.

We now go on to consider the possible effects of colour coherence in two jet events at the Tevatron collider. For example, by crossing Eq.(8), we can show that the antenna pattern function for the process,

$$q(p_1) + \bar{q}'(p_2) \rightarrow q(p_3) + \bar{q}'(p_4) \quad (35)$$

is given by,

$$P\left(\frac{t}{s}, \frac{u}{s}; \theta, \phi\right) = \frac{C_F}{4N} \left(\frac{\zeta_{12}}{\zeta_1\zeta_2} + \frac{\zeta_{34}}{\zeta_3\zeta_4} \right) + \frac{1}{8N^2} \left(2 \frac{\zeta_{14}}{\zeta_1\zeta_4} + 2 \frac{\zeta_{34}}{\zeta_3\zeta_4} - \frac{\zeta_{13}}{\zeta_1\zeta_3} - \frac{\zeta_{24}}{\zeta_2\zeta_4} - \frac{\zeta_{12}}{\zeta_1\zeta_2} - \frac{\zeta_{34}}{\zeta_3\zeta_4} \right). \quad (36)$$

In this case the antenna function has a particularly simple form because Eq. (16) is proportional to the lowest order cross-section. The principal two-to-two scattering processes responsible for jet production in $p\bar{p}$ collisions are,

$$\begin{aligned} q(p_1) + \bar{q}(p_2) &\rightarrow q(p_3) + \bar{q}(p_4) \\ g(p_1) + q(p_2) &\rightarrow g(p_3) + q(p_4) \\ g(p_1) + g(p_2) &\rightarrow g(p_3) + g(p_4). \end{aligned} \quad (37)$$

The antenna patterns for these processes are easily derived from Eqs. (19,20,21) and Table I. Figs. 10, 11 and 12 show the resulting antenna patterns for the 90° scattering in the centre of mass. It can be seen from Fig. 11 that in $qg \rightarrow qg$ there is an asymmetry of about a factor four between the first and the third quadrant, which, if detectable, would allow the identification of gluon and quark jets on an event by event basis. By moving to large rapidity we select events in which the fraction of the longitudinal momentum of the hadron carried by one of the partons is very large and the other is very small, leading to an enhanced contribution from quark-gluon scattering. Fig. 13 shows the enrichment of the qg fraction which can be achieved by moving to large rapidity. We have chosen $y_1 = y_2$ corresponding to 90° scattering in the centre of mass and adopted a notional value of $p_T = 90$ GeV. At $y = 1$ the qg fraction is 44% rising slowly to 60% at $y = 2$. Since it is not possible to obtain a pure sample of qg events, the fluctuations of qg and gg events into asymmetrical configurations may provide serious contamination of the qg sample. Nevertheless the prospect of identifying quark and gluon jets in the same event is sufficiently exciting that the problem deserves further study.

Acknowledgements

I would like to thank A. H. Mueller and G. Marchesini for discussions and E. J. Eichten for assistance in calculating the jet cross-sections of Fig. 13.

References

- [1] For a review see A. Kernan and G. VanDalen, *Phys. Rep.* **106** (1984) 298 ;
J. L. Ritchie, in *Proc. 1984 Summer Study on the Design and Utilization of the Superconducting Super Collider*, R. Donaldson and J. Morfín, (eds.), Fermilab, Batavia, Illinois, 1984, p. 237, and references therein.

- [2] J. P. Albanese et al., *Phys. Lett.* **158B** (1983) 51 ;
M. G. Catanesi et al., *Phys. Lett.* **187B** (1987) 431 ;
C. Albajar et al., *Phys. Lett.* **186B** (1987) 237 .
- [3] M. Purohit, these proceedings.
- [4] J. C. Collins, D. E. Soper, and G. Sterman, *Nucl. Phys.* **B263** (1986) 37 ;
P. Mazzanti and S. Wada, *Phys. Rev.* **D26** (1982) 602 .
- [5] S. J. Brodsky, J. C. Collins, S.D. Ellis, J. F. Gunion and A. H. Mueller, in *Proc. 1984 Summer Study on the Design and Utilization of the Superconducting Super Collider*, R. Donaldson and J. Morfin, (eds.), Fermilab, Batavia, Illinois, 1984, p. 227.
- [6] R. K. Ellis, in *Strong Interactions and Gauge Theories*, edited by J. Tran Thanh Van, Editions Frontières, Gif-sur-Yvette, 1986, p. 339.
- [7] R. K. Ellis and J. C. Sexton, *Nucl. Phys.* **B282** (1987) 642 .
- [8] J. F. Gunion and Z. Kunszt, *Phys. Lett.* **178B** (1986) 296 ;
Z. Kunszt and E. Pietarinen, *Nucl. Phys.* **B164** (1980) 45 ;
T. Gottschalk and D. Sivers, *Phys. Rev.* **D21** (1980) 102 .
- [9] F. A. Berends, R. Kleiss, P. de Causmaecker, R. Gastmans and T. T. Wu, *Phys. Lett.* **103B** (1981) 102 .
- [10] B. L. Combridge, *Nucl. Phys.* **B151** (1979) 4299 .
- [11] J. Babcock, D. Sivers and S. Wolfram, *Phys. Rev.* **D18** (1978) 162 .
- [12] K. Hagiwara and T. Yoshino, *Phys. Lett.* **80B** (1979) 282 ;
L. M. Jones and H. Wyld, *Phys. Rev.* **D17** (1978) 782 ;
H. Georgi et al., *Ann. Phys. (NY)* **114** (1978) 273 .
- [13] C. Quigg, "b \bar{b} Production in Tevatron II Experiments," memorandum, July, 1985 (unpublished).
- [14] R. K. Ellis and C. Quigg, Fermilab preprint FN-445 (1987).
- [15] J. F. Owens, *Phys. Rev.* **D30** (1984) 983 .
- [16] D. W. Duke and J. F. Owens, *Phys. Rev.* **D30** (1984) 49 .
- [17] For a review see: A. Bassetto, M. Ciafaloni and G. Marchesini, *Phys. Rep.* **100** (1983) 201 .
- [18] A. H. Mueller, *Phys. Lett.* **104B** (1981) 161 , *Nucl. Phys.* **B213** (1983) 85 , *Nucl. Phys.* **B241** (1984) 141 .
- [19] A. Bassetto, M. Ciafaloni , G. Marchesini and A. H. Mueller, *Nucl. Phys.* **B207** (1982) 189 .
- [20] B. I. Ermolaev and V. S. Fadin, *JETP Lett.* **33** (1981) 285.

- [21] H. Yamamoto, Report at the International Symposium on Lepton and Photon Interactions at High Energy, Kyoto (1985).
B. Andersson, G. Gustafsson, G. Ingelman and T. Sjöstrand *Phys. Rep.* **97** (1983) 33 .
- [22] Ya. I. Azimov, Yu. L. Dokshitzer, V. A. Khoze and S. Troyan, *Phys. Lett.* **165B** (1985) 147 .
- [23] G. Marchesini and B. R. Webber, work in progress.
- [24] S. Catani, M. Ciafaloni and G. Marchesini, *Nucl. Phys.* **B264** (1986) 588 ;
M. Ciafaloni, Proceedings of the 23rd International Conference on High Energy Physics, Berkeley, California (1986).
- [25] G. Marchesini and B. R. Webber, *Nucl. Phys.* **B238** (191984) 1 ;
B. R. Webber, *Nucl. Phys.* **B238** (1984) 492 .
- [26] T. Sjöstrand, Lund preprint, LU TP 85-10 (1985).
- [27] For a review see: B. R. Webber *Ann. Rev. Nucl. Part. Sci.* **36** (1986) 253 .
- [28] B. R. Webber, Proc. XV Symposium on Multiparticle Dynamics, Lund (1984), p. 627;
Proc. XVI Symposium on Multiparticle Dynamics, Kiryat Anavim (1985), p. 41.
- [29] T. Sjöstrand, *Phys. Lett.* **157B** (1985) 321 ;
T. D. Gottschalk, Caltech preprint, CALT-68-1241 (1985).
- [30] R. K. Ellis, G. Marchesini and B. Webber, *Nucl. Phys.* **B286** (1987) 643 (Fermilab preprint Pub-86/141-T).
- [31] R. K. Ellis and R. J. Gonsalves, Proceedings of the Oregon Workshop on Super High Energy Physics, p. 287, World Scientific.
- [32] G. Altarelli and G. Parisi, *Nucl. Phys.* **B126** (1977) 298.
- [33] Yu. L. Dokshitzer, V. A. Khoze and S. I. Troyan, Leningrad preprint 1218 (1986).
- [34] Yu. L. Dokshitzer, V. A. Khoze, S. I. Troyan and A. H. Mueller, Columbia preprint CU-TP-374 (1987).
- [35] Ya. I. Azimov, Yu. L. Dokshitzer, V. A. Khoze and S. I. Troyan, *Sov. J. Nucl. Phys.* **43** (1986) 95 .
- [36] M. Althoff et al., *Zeit. Phys.* **C17** (1983) 5 .
- [37] G. J. Alner et al., *Zeit. Phys.* **C33** (1986) 1 .

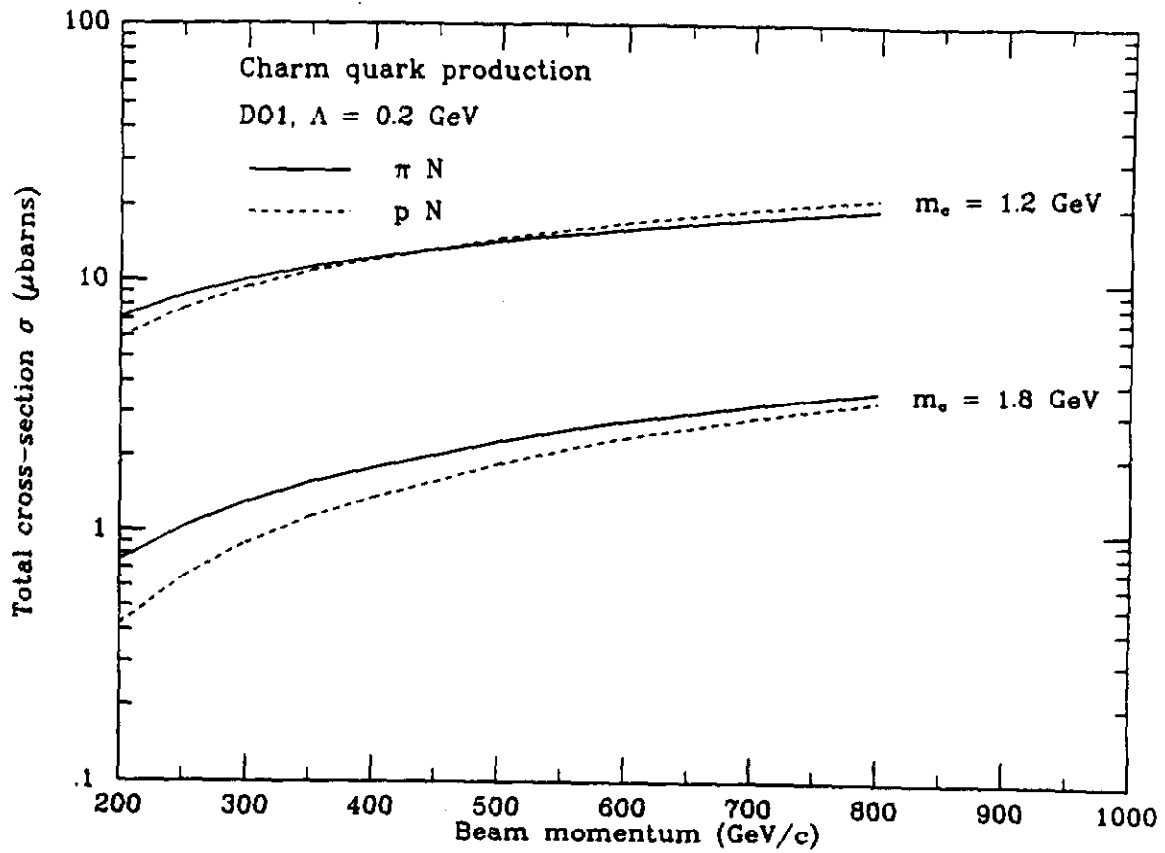


Figure 1: Integrated cross sections for the production of charmed quarks in πN (solid lines) and pN (dashed lines) collisions as a function of the beam energy.

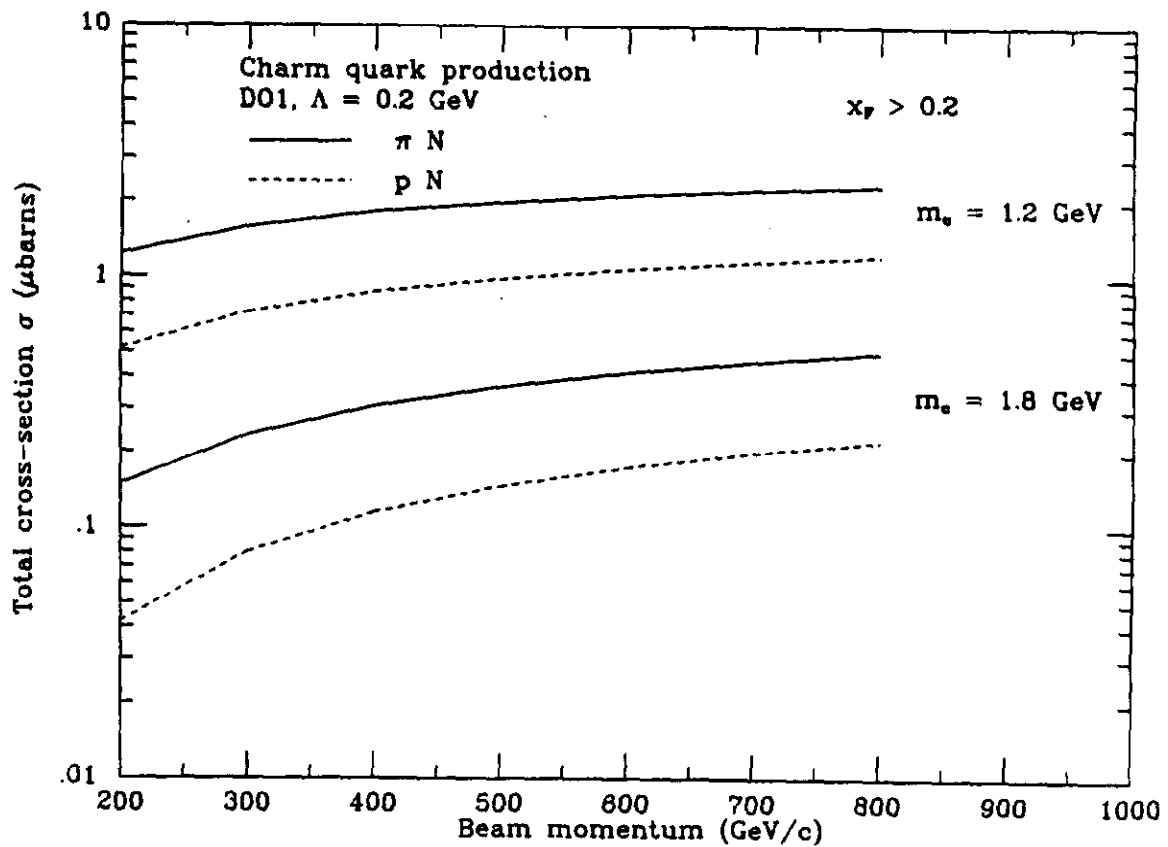


Figure 2: Integrated cross sections for the forward production ($x_F > 0.2$) of charmed quarks in πN (solid lines) and pN (dashed lines) collisions.

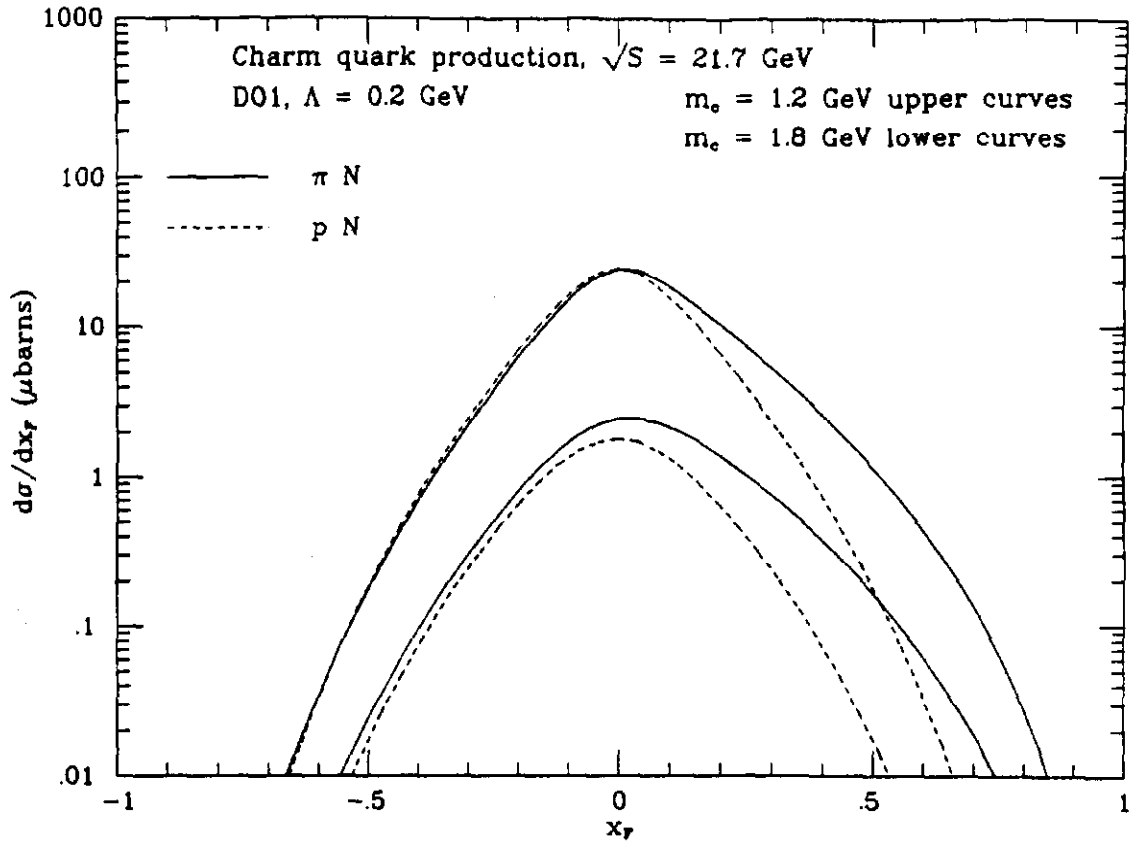


Figure 3: Differential cross section $d\sigma/dx_F$ for the production of charmed quarks in πN (solid lines) and pN (dashed lines) collisions at $\sqrt{S}=21.7$ GeV ($p_{\text{beam}}=250$ GeV).

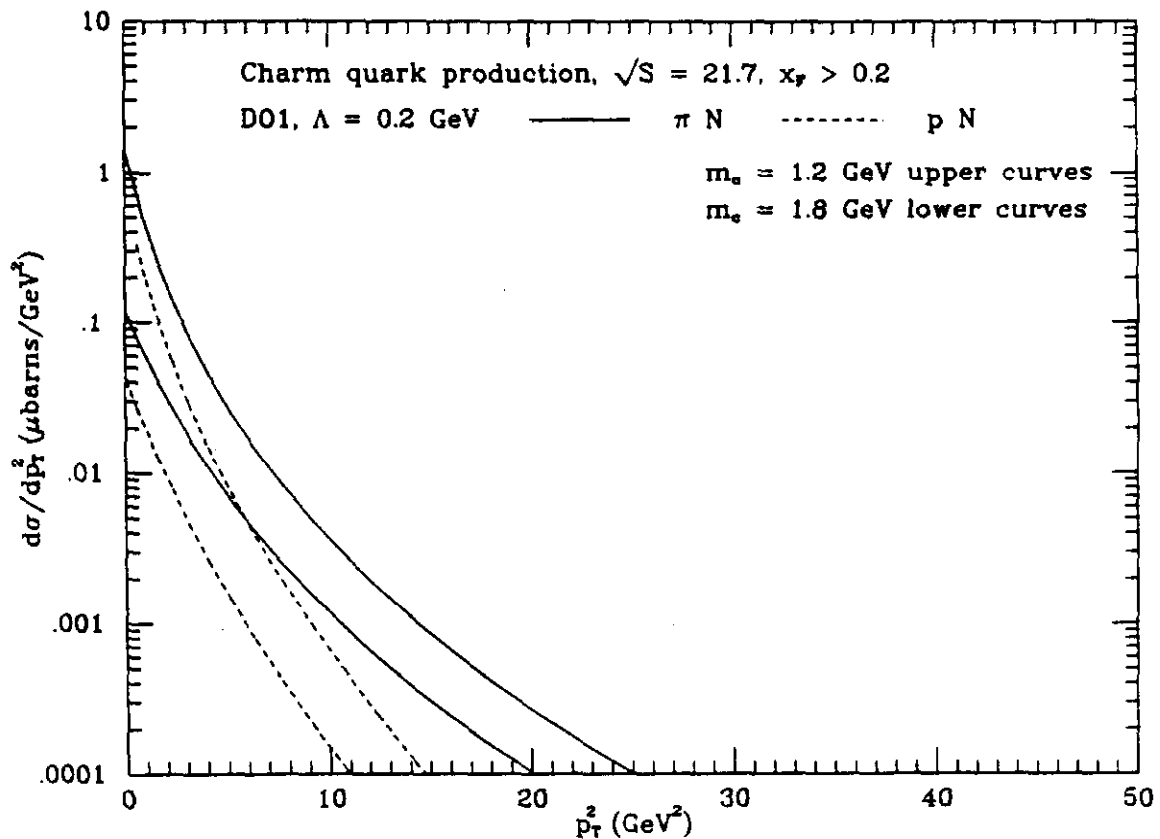


Figure 4: Differential cross section $d\sigma/dp_T^2$ for the production of charmed quarks in the forward region ($x_F > 0.2$) in πN (solid lines) and pN (dashed lines) collisions at $\sqrt{S}=21.7$ GeV

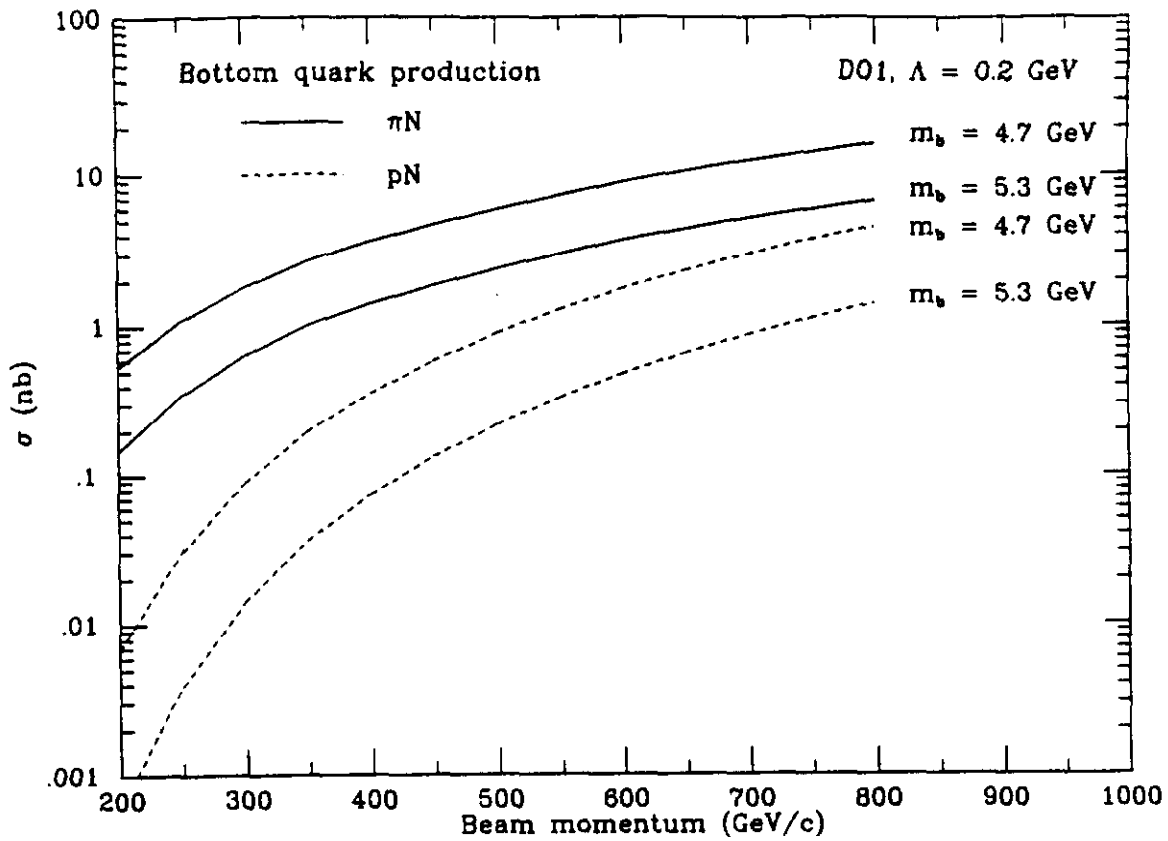


Figure 5: Integrated cross sections for the production of bottom quarks in πN (solid lines) and pN (dashed lines) collisions as a function of the beam energy.

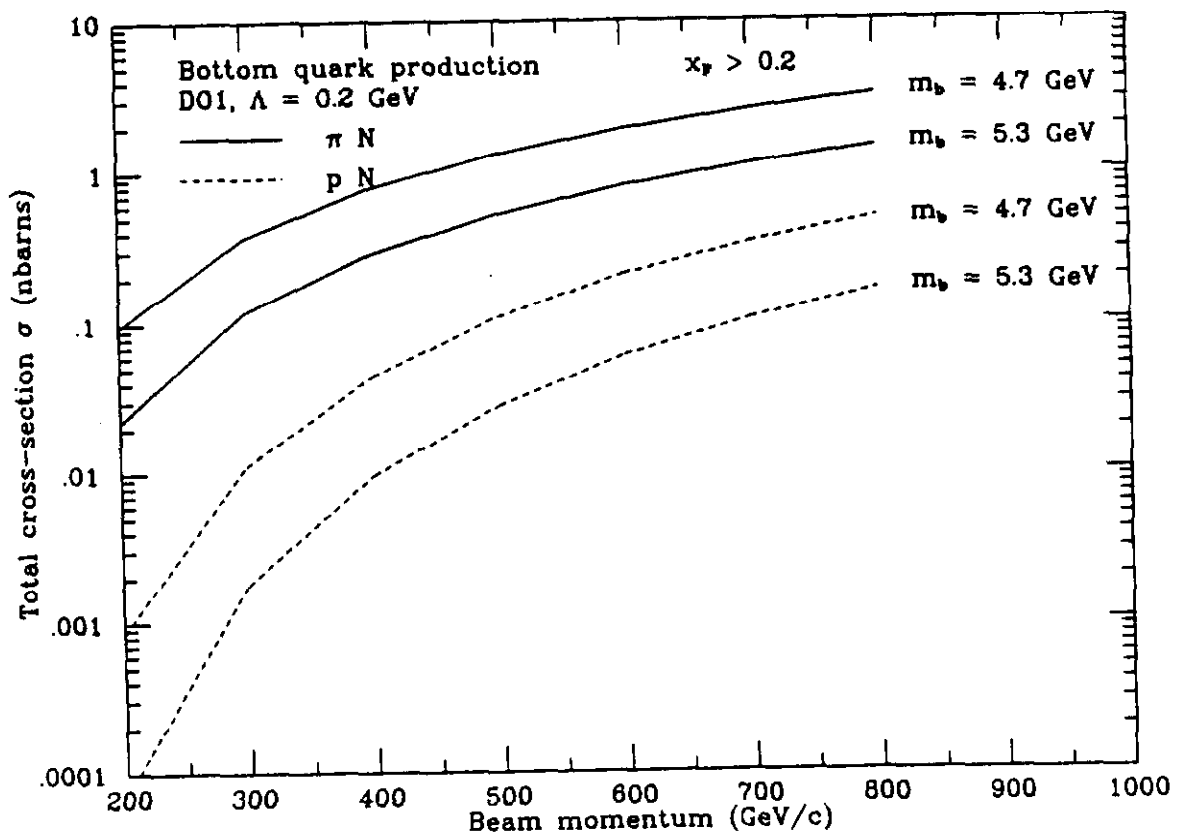


Figure 6: Integrated cross sections for the forward production ($x_F > 0.2$) of bottom quarks in πN (solid lines) and pN (dashed lines) collisions.

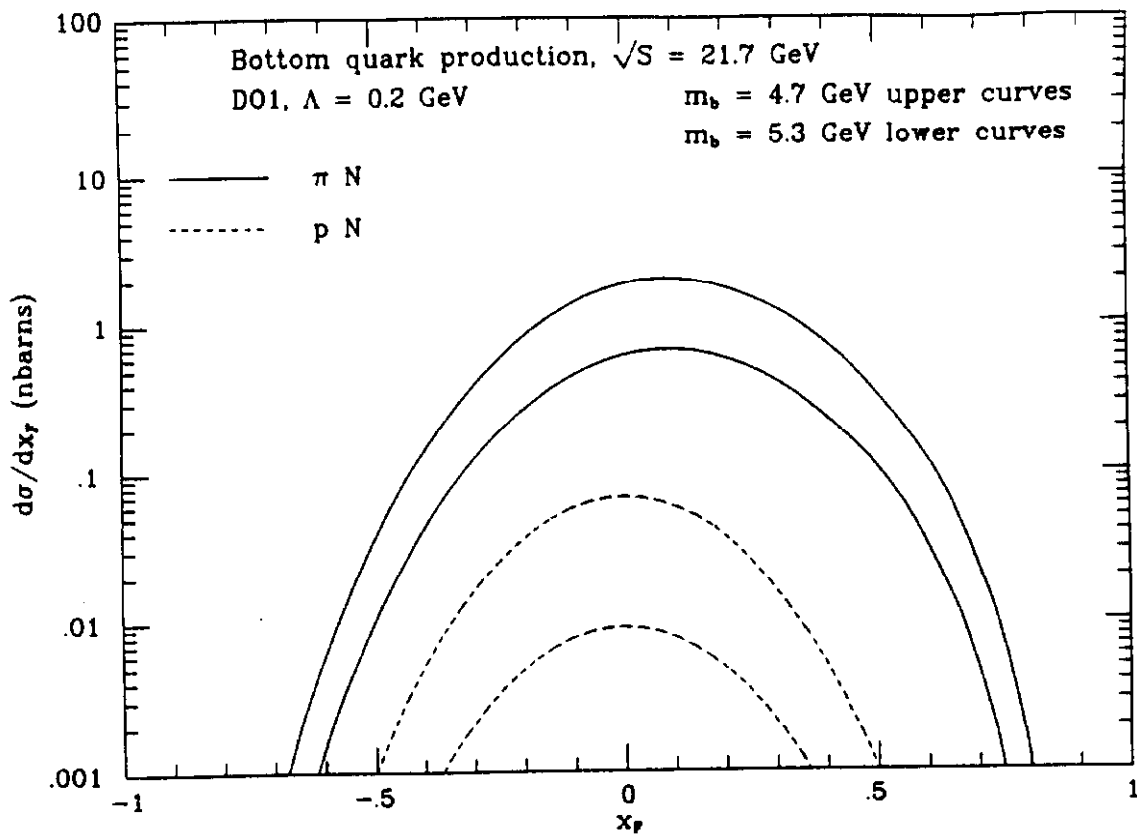


Figure 7: Differential cross section $d\sigma/dx_F$ for the production of bottom quarks in πN (solid lines) and pN (dashed lines) collisions at $\sqrt{S}=21.7$ GeV ($p_{beam}=250$ GeV).

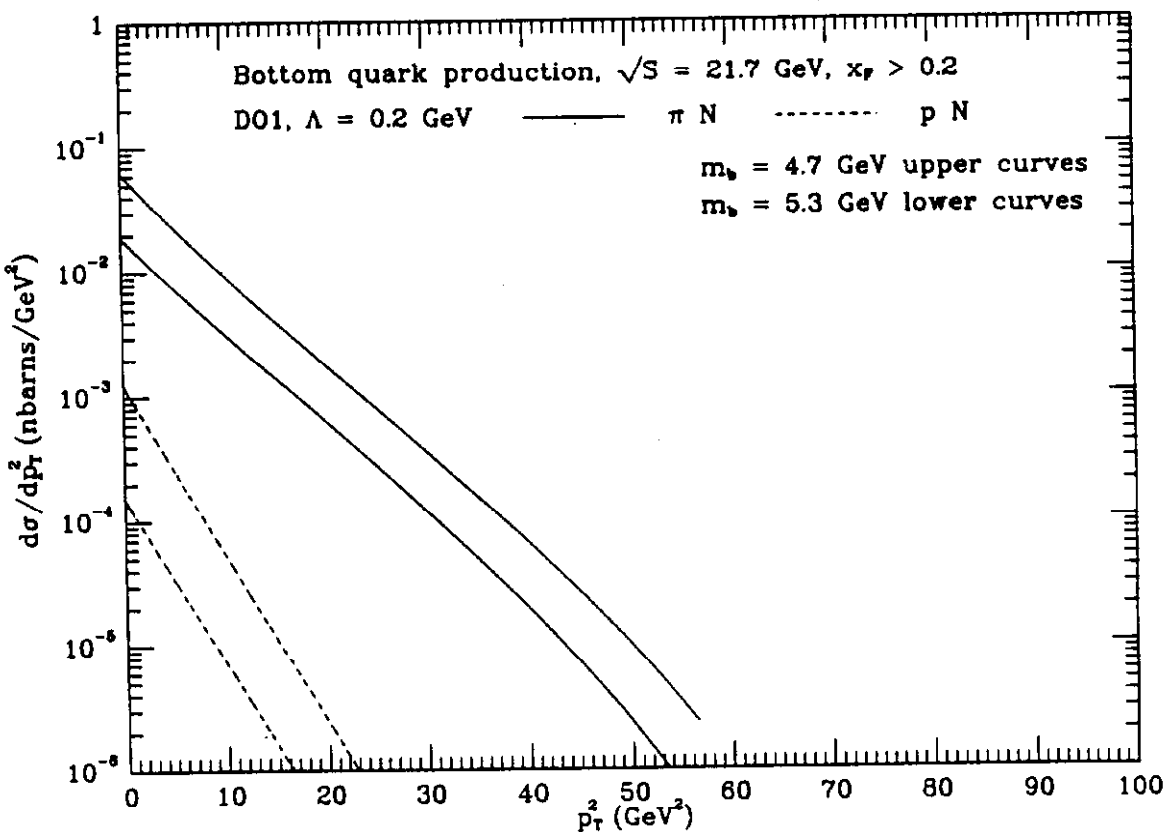


Figure 8: Differential cross section $d\sigma/dp_T^2$ for the production of bottom quarks in the forward region ($x_F > 0.2$) in πN (solid lines) and pN (dashed lines) collisions at $\sqrt{S}=21.7$ GeV

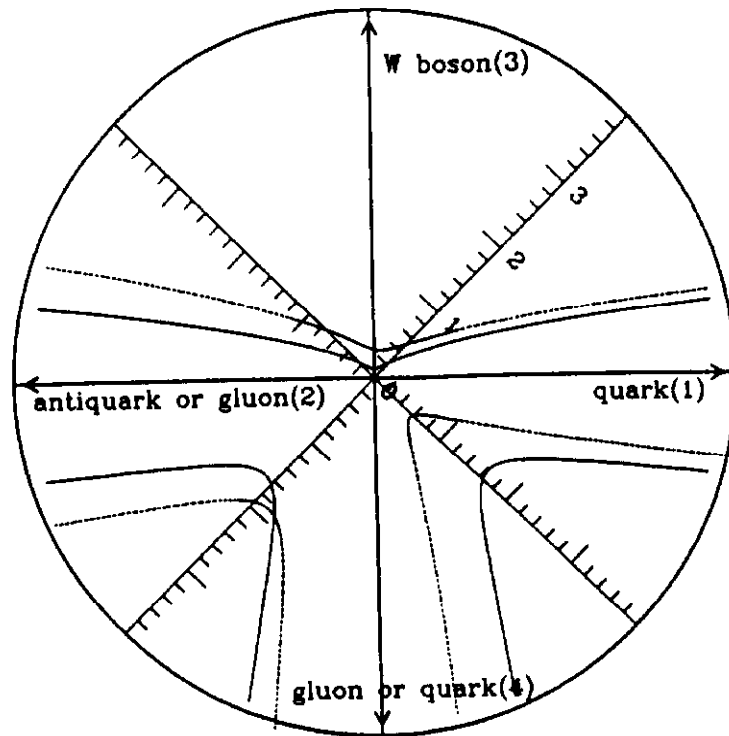


Figure 9: Polar plot showing the antenna pattern $P(-\frac{1}{2}, -\frac{1}{2}; \theta, 0)$ versus θ for the processes $q(p_1) + \bar{q}(p_2) \rightarrow W(p_3) + g(p_4)$, (solid line) and $q(p_1) + g(p_2) \rightarrow W(p_3) + q(p_4)$, (dashed line) for 90° scattering in the centre of mass. The value of P is given by the radial distance of the curves from the origin. The plots have been cut off at $P = 4$, so the singularities in the collinear regions are not displayed.

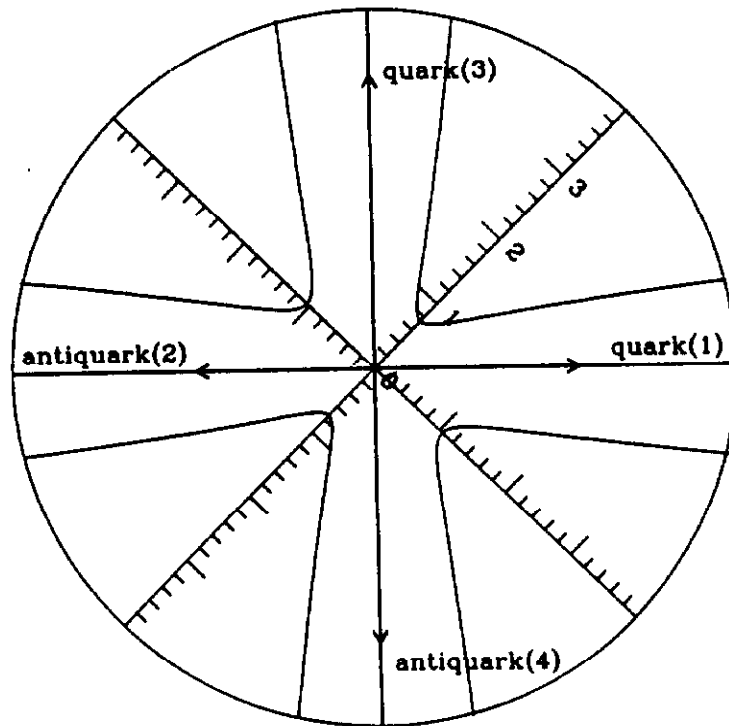


Figure 10: Polar plot showing the antenna pattern $P(-\frac{1}{2}, -\frac{1}{2}; \theta, 0)$ versus θ for the identical quark process $q(p_1) + \bar{q}(p_2) \rightarrow q(p_3) + \bar{q}(p_4)$.

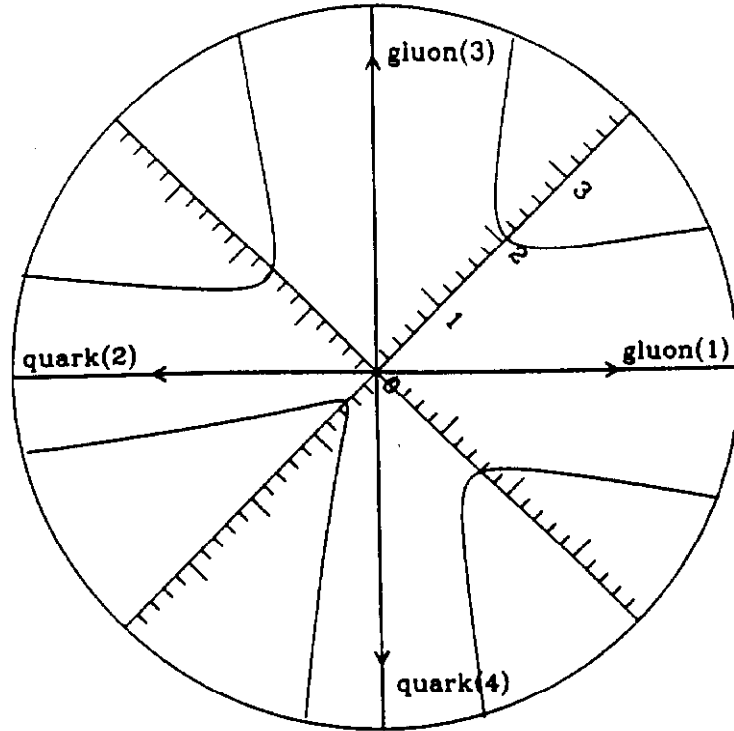


Figure 11: Polar plot showing the antenna pattern $P(-\frac{1}{2}, -\frac{1}{2}; \theta, 0)$ versus θ for the process $g(p_1) + q(p_2) \rightarrow g(p_3) + q(p_4)$.

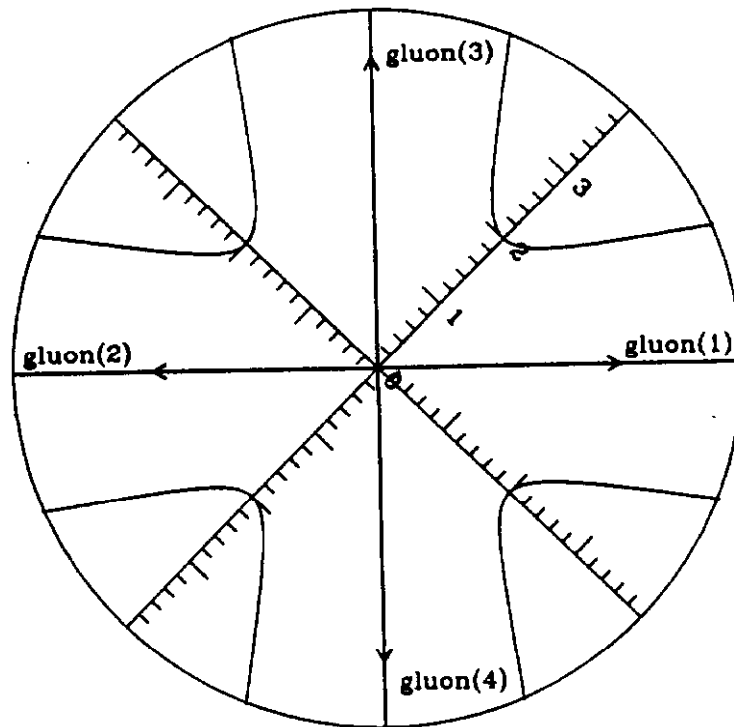


Figure 12: Polar plot showing the antenna pattern $P(-\frac{1}{2}, -\frac{1}{2}; \theta, 0)$ versus θ for the process $g(p_1) + g(p_2) \rightarrow g(p_3) + g(p_4)$.

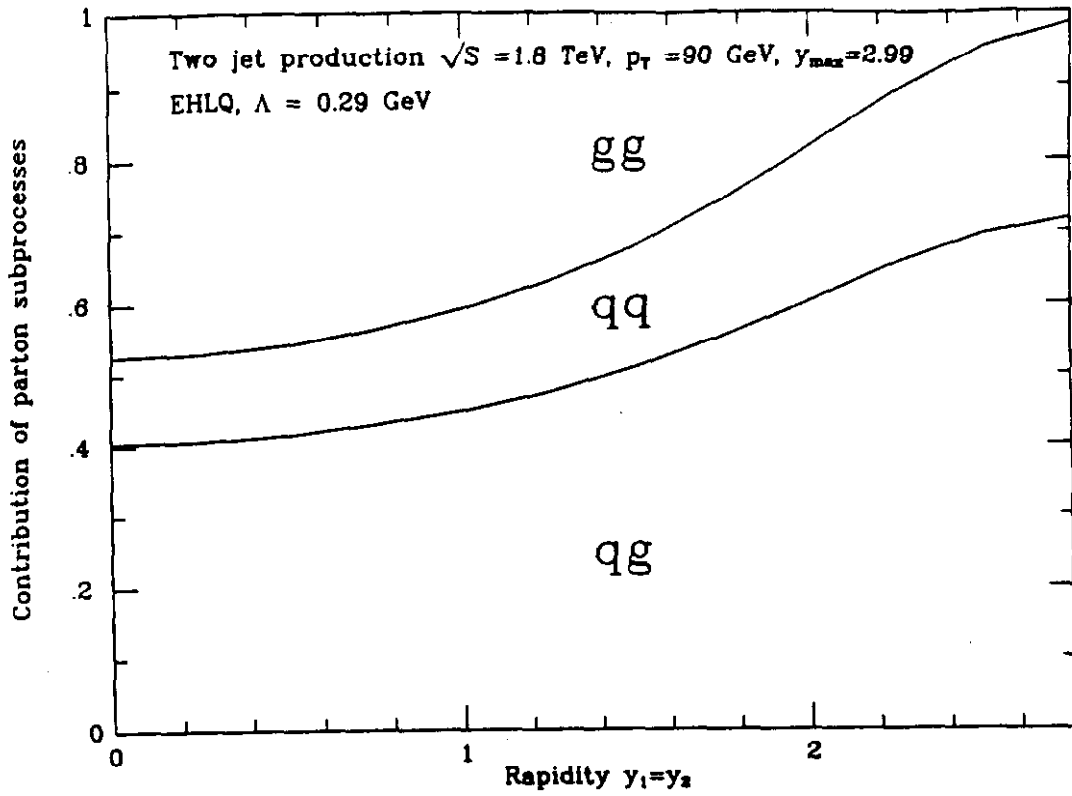


Figure 13: Fractional contributions of the various subprocesses (indicated by the size of the three regions in the plot) in large p_T scattering at $\sqrt{S}=1.8$ TeV as a function of the hadron-hadron centre of mass rapidity of the two jets $y_1 = y_2$.